Nesting the Gulf of Mexico in Atlantic HYCOM: Oceanographic processes generated by Hurricane Ivan

Luis Zamudio [a],[*], Patrick J. Hogan [b]

[a] *Center for Ocean-Atmospheric Prediction Studies, Florida State University, Tallahassee, FL 32306-2840, United States*
[b] *Naval Research Laboratory, Stennis Space Center, MS, United States*

Abstract

The HYbrid Coordinate Ocean Model (HYCOM) has been configured for the Gulf of Mexico (GOM) at 1/25° horizontal grid resolution and has been nested inside a basin-scale 1/12° Atlantic version of HYCOM. The 1/25° nested GOM model is used to study temperature variations, current patterns, transport variations, and two coastal-trapped waves (CTWs) generated by Hurricane Ivan during mid September 2004. The model results indicate that the winds generated by Ivan: (1) induced a transport variation of approximately 2 Sv/day along the Yucatan Channel, (2) enhanced the oceanic mixing lowering the sea surface temperature more than 3 °C along Ivan's path, (3) produced a thermocline vertical velocity of >100 m/day, and (4) generated a westward transport of ~8 Sv along the northern coast of the GOM that was redirected by the Louisiana coastline inducing a southward transport of ~6 Sv. Throughout its passage over the Caribbean Sea Ivan generated first a CTW along the south east coast of Cuba. After its generation this wave propagated along the coast and partially propagated along the western tip of the Cuban Island and continued its propagation along the northern coast of the Island. The model existence of CTWs along the coast of Cuba is reported for the first time. Later on, over the Florida–Alabama–Mississippi–Louisiana coast, Ivan's westward winds drove a model oceanic onshore transport and generated a strong coastal convergence. The convergence raised the sea surface height ~90 cm generating a second CTW, which is characterized by alongshore and cross-shore scales of ~700 and ~80 km, respectively. The CTW current pattern includes westward surface currents of more than 2.0 m/s. After its generation, the wave weakened rapidly due to Ivan's eastward winds, however a fraction of the CTW propagated to the west and was measured by a tide gauge at Galveston, Texas. The descriptions, hypothesis, and discussions presented in this study are based on model results and those results are compared and validated with sea surface height coastal tide gauge observations and sea surface temperature buoy observations.
Published by Elsevier Ltd.

1. Introduction

The cyclone that became Ivan was classified as a tropical depression on September 2, 2004. At that time the cyclone was located in the middle of the Tropical Atlantic Ocean near 29.10°W–9.70°N and featured maximum sustained winds of ~13 m/s. During the following two weeks Ivan traveled through the Caribbean Sea and the GOM strengthening its maximum sustained winds to ~75 m/s, and generating wind waves with amplitude of ~27 m in the northern GOM (http://www.nhc.noaa.gov; Wang et al., 2005).

Ivan entered into the GOM on September 14, 2005, with wind speeds >60 m/s through the Yucatan channel (Fig. 1) providing strong wind-forcing for both the real GOM ocean and the GOM numerical ocean models, supplying surface boundary conditions for those models, and challenging the GOM models to accurately simulate the response to the strong and rapidly propagating Ivan wind system. The results of this study show that: (1) Two CTWs were generated by Hurricane Ivan. One of them was generated along the coast of Cuba and the other along the Florida–Alabama–Mississippi–Louisiana coast. The model generation of a CTW along the coast of Cuba is reported for the first time. (2) GOM buoys recorded sea surface temperature (SST) decreases of >3 °C in ~2 days as an upper ocean

Corresponding author.
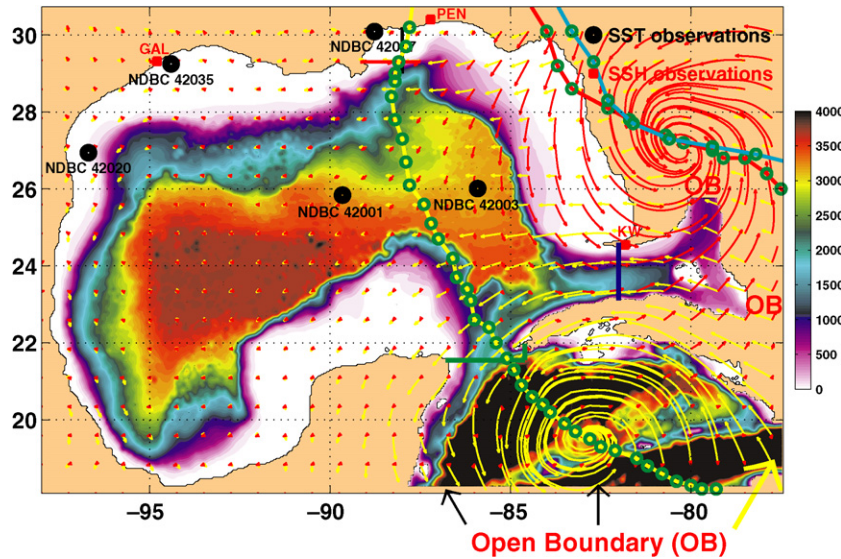 *E-mail address:* Luis.Zamudio@nrlssc.navy.mil (L. Zamudio).

Fig. 1. The color contours represent the bottom topography (in meters) of the regional Gulf of Mexico model. The path of Frances, Ivan, and Jeanne are represented with red, cyan, and yellow lines with open green circles, respectively. The four open boundaries, which communicate with the basin scale Atlantic HYCOM are indicated with OB. The black circles represent the location of the NOAA buoys (which are identified with the National Data Buoy Center (NDBC) station number) where the sea surface temperature (SST) measurements are taken. The red squares represent the position of tide gauges at Key West (KW), Pensacola (PEN), and Galveston (GAL) where the sea surface height (SSH) measurements are taken. The transports are calculated along the green line in the Yucatan Channel (Fig. 4), along the blue line from Key West to Cuba (Fig. 4), along the red line from the Coast of Louisiana to 87.52°W, 29.31°N (Fig. 14), and along the black line from the Coast of Mississippi to 88.00°W, 29.00°N (Fig. 14). The red (yellow) curly vectors represent Hurricane Frances (Ivan) winds during September 5 (13), 2004.

response to Ivan's winds. That strong and rapid ocean reaction to the Hurricane wind forcing is an excellent test case to examine the capabilities of mixed layer sub-models to simulate rapid cooling events. Thus five different mixed layer sub-models (which are embedded in HYCOM) were used to investigate the SST evolution during the year 2004. (3) The deterministic (which is considered here as the direct response to atmospheric and remote forcings), and nondeterministic (which is attributed to nonlinear mesoscale flow instabilities) regions of the GOM are calculated and are used to explain the differences between modeled and observed sea surface height.

2. Model

2.1. HYCOM configurations

HYCOM is the HYbrid vertical Coordinate Ocean Model, which is isopycnal in the open stratified ocean, terrain-following in shallow coastal regions, and z-level in mixed layer and unstratified regions. This generalized vertical coordinate approach is dynamic in space and time via the layered continuity equation that allows a smooth dynamical transition between the coordinate types. HYCOM (Bleck, 2002) was developed from the Miami Isopycnic Coordinate Ocean Model (MICOM) using the theoretical foundation for implementing a hybrid coordinate system (Bleck and Benjamin, 1993). Since a single vertical

coordinate (depth, density, or terrain-following sigma) cannot by itself be optimal everywhere in the ocean, the hybrid approach of HYCOM is an option, which uses the optimal of the three vertical coordinates depending on the ocean characteristics. For instance, isopycnal (density tracking) layers are best in the deep stratified ocean, z-levels (constant fixed depths) are best used to provide high vertical resolution near the surface within the mixed layer (and other unstratified regions), and σ-levels (terrain-following) are often the best choice in shallow coastal regions (Chassignet et al., 2000, 2007; Willebrand et al., 2001).

The eddy-resolving (1/12° equatorial resolution) basin scale Atlantic HYCOM domain extends from 27.9°S to 70.0°N and from 98.0°W to 36.2°E, and the 1/25° nested regional GOM-HYCOM domain extends from 98°W to 77.4°W and from 18°N to 31°N. The two HYCOM configurations are identically forced with 3-hourly winds and daily averaged heat fluxes from the Fleet Numerical Meteorology and Oceanography Center's Navy Operational Global Atmospheric Prediction System (NOGAPS) (Rosmond et al., 2002), and they include monthly mean values for rivers and turbidity forcing (Kara et al., 2005a–c). A previous non-assimilative Atlantic HYCOM simulation was integrated to statistical equilibrium using climatological monthly winds, and it was then continued using 3-hourly winds to ultimately provide initial conditions for the Atlantic simulation used in this study. Atlantic HYCOM ran from May 2003 to October 2007 whereas the nested GOM-HYCOM simulations are only integrated

over year 2004. Initial conditions for GOM-HYCOM were provided by Atlantic HYCOM. In addition, the models include realistic bottom topography and coastline geometry that are based on a modified version of the 1/30° NRL DBDB2 topography (http://www.7320.nrlssc.navy.-mil/DBDB2_WWW). The models use the 5 meter isobath as a land-sea boundary, and allow isopycnals intersecting sloping topography by allowing zero thickness layers. Atlantic HYCOM includes 26 vertical layers and assimilation of satellite measured sea surface height (SSH) and SST data (http://www.7320.nrlssc.navy.mil/ATLhycom1-12/skill.html), while GOM-HYCOM includes 20 vertical coordinate layers and does not include ocean data assimilation. Furthermore, both Atlantic and GOM-HYCOM include five different embedded ocean mixed layer sub-models that can be used to simulate the variability of the mixed layer. Those models are the K-Profile Parameterization (Large et al., 1994), the NASA Goddard Institute for Space Studies (Canuto et al., 2001, 2002) turbulence closure, the Mellor–Yamada (Mellor and Yamada, 1982) turbulence closure, the Krass–Turner (Turner and Kraus, 1967; Niiler and Kraus, 1977) bulk mixed layer model, and the Price–Weller–Pinkel (Price et al., 1986) mixed layer model (Halliwell, 2004). HYCOM simulations with and without an embedded mixed layer sub-model are presented and discussed in Section 3.

2.2. Nesting with HYCOM

Details about the HYCOM nesting procedure have been reported in the HYCOM USER GUIDE (Wallcraft, 2003, available at http://hycom.rsmas.miami.edu/hycom-model/documentation.html). Here some general features of the procedure are mention. Nesting within HYCOM is a one-way (from the larger domain to the nested domain) off-line process. Thus, the user can define (after the fact) any nested domain that lies within the outer model. However, this nesting approach has the disadvantage of limiting the updating frequency of the boundary conditions for the nested domain to the frequency of the results archived from the outer model. During the nesting process the baroclinic modes are relaxed to the coarse outer grid solution via a relaxation buffer zone for temperature, salinity, pressure and horizontal velocity components. The barotropic mode is passed into the inner domain along characteristic lines for velocity and pressure. There are several nesting parameters, which may be tuned for optimal passage of oceanic signals across the open boundary. These include the updating frequency at the boundary, the number of grid points to be included in the relaxation buffer zone, the relaxation time across the buffer zone, and the effect of excluding the baroclinic or barotropic mode from the boundary conditions. The nesting parameters used in this study are: the boundary conditions updated every 1-day, the relaxation buffer zone includes 20 grid points, the relaxation time across the buffer zone of 1–10 days, and the barotropic and baroclinic modes included in the nested boundary conditions.

3. Results and discussion

The description and discussion presented in this section is based on model results and the model results are compared and validated with SSH coastal tide gauge observations and SST buoy observations.

3.1. Hurricane Ivan in the Northwestern Caribbean Sea

3.1.1. Volume transport response to the passage of Hurricane Ivan

Before the arrival of Hurricane Ivan to the Northwestern Caribbean the surface currents along the Yucatan Channel were characterized by the Yucatan Current flowing into the Gulf of Mexico, with its core of >130 cm/s located on the western part of the channel, and by the Cuban Counter-current positioned on the eastern side of the channel (Fig. 2a). On this particular day (September 9, 2004) the maximum of the Cuban Counter-current (>45 cm/s) is not attached to the Cuban coast, and this counter-current is weakened by a northward flow, which is represented by the yellow contours near the Cuban coast in Fig. 2a. Although September 9 is just a snapshot of a summer day in the Yucatan Channel, the instantaneous currents produced by the model resemble the basic structure of the observed mean currents (e.g. Sheinbaum et al., 2002). During the same day, the currents across the Western Florida Strait (from Key West to Cuba) are characterized by the eastward flowing Florida Current, which has a surface maximum of >105 cm/s located in the northern part of the strait, a weak westward counter-flow beneath it, and a weak surface counter-flow attached to the southern coast of the strait (Fig. 3a). This HYCOM simulated Florida Current also reproduces the main features of the observed currents in the region (e.g. Hamilton et al., 2005).

The GOM-HYCOM simulated currents across the Yucatan Channel and Western Florida Strait Channels are strongly altered by the passage of Hurricane Ivan over the Northwestern Caribbean. In particular, Hurricane Ivan: (1) reversed the direction of the Cuban Counter-Current (from southward to northward) generating a maximum northward flow of >210 cm/s. This hurricane induced maximum flow is located on the eastern part of the Channel (with center close to 85°W in Fig. 2b) and modified the mean current pattern, which is well known to have a maximum on the western side. (2) Generated a maximum mixed layer thickness of ~200 m on the eastern part of the channel (as denoted by the black line in Fig. 2b), and (3) created a significant change in the across channel mixed layer thickness from ~20 m on September 9 to ~100 m on September 14 (again denoted by the black line in Figs. 2a and b). In the Western Florida Strait, model results show that maximum current speed increased from >105 cm/s on September 9 to >165 cm/s on September 15 (Fig. 3a and b), and the location of the current and mixed layer thickness maxima changed from the northern part of
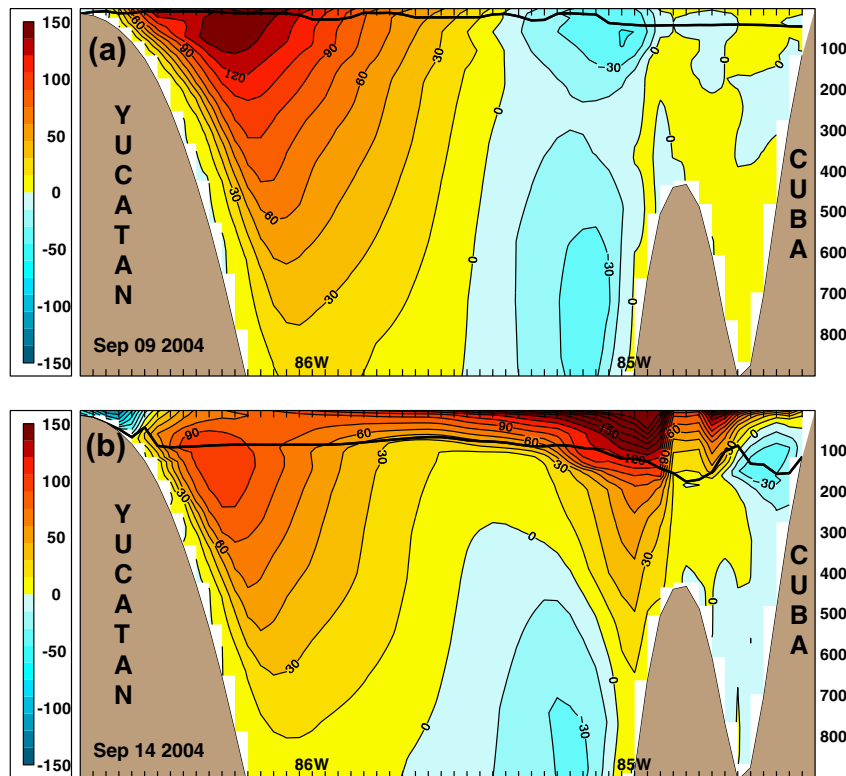
Fig. 2. North–South component of the velocity (color contours in cm/s) snapshots for September 9, 2004 (a) and September 14, 2004 (b) as simulated by the 1/25° nested GOM-HYCOM over a cross-section along the Yucatan Channel, which is indicated with a green line in Fig. 1. Positive currents indicate northward flow. The mixed layer depth is represented by the black line.

the strait on September 9 to the southern part of the strait on September 15, all produced by the passage of Ivan. How does the hurricane generated currents affect the transport across the Yucatan Channel and Western Florida Strait? A plausible answer to this question is discussed in the next paragraph.

Since the GOM has just one entrance (the Yucatan Channel) and one exit (the Western Florida Strait), over time scales of days the imbalance in volume storage in the GOM is close to zero (Bunge et al., 2002). Hence, the northward Yucatan Channel inflow must be rapidly compensated, nearly as a mirror image, by the eastward Western Florida Strait outflow at any given time. Over 2004 that is illustrated by the two transport time-series of Fig. 4a, which demonstrate the balance in volume storage. A relevant feature of these time series is the significant reduction in transport that occurred during late march, which reached a minimum of ~20 Sv. According to North Atlantic HYCOM results, which provide boundary conditions for GOM-HYCOM, this transport reduction was remotely originated by fluctuations in the North Brazilian Current. Of particular interest for this study is the impact of Hurricane Ivan on the Yucatan Channel transport. Thus, Fig. 4b is a close up of Fig. 4a for the month of September 2004. The effects of Hurricanes Frances and Ivan on the transport are the two most significant features of Fig. 4b. When Hurricane Ivan was approaching the

GOM, the winds in the Yucatan Channel changed from basically no wind on September 10–11, to augmented southwestward wind on September 12–13, to strong southward (northward) wind in the eastern (western) part of the channel on September 14, to strong northward wind on September 15, and finally to relaxed winds after that (Fig. 5). Those wind variations generated first (second) a reduction (augmentation) of the Yucatan Channel northward transport that reached a minimum (maximum) of ~26 (~32) Sv on September 14 (17) (Fig. 4b). Thus, the maximum Yucatan Channel transport variation, and consequently the Western Florida Strait transport variation, due to the passage of Hurricane Ivan, is ~2 Sv/day. In the GOM oceanographic literature it is well accepted that the transport through the Caribbean and the Yucatan Channel is supplied by the Western Subtropical Atlantic and the South Atlantic via the North Brazilian Current (Schott et al., 1993; Johns et al., 1998). Thus, remotely forced variations in the North Brazilian Current can produce fluctuations in the Yucatan Channel transport (Fig. 4). Also, in a local perspective, Lee et al. (1995) and Hamilton et al. (2005) reported transport's reduction along the Western Florida Strait due to the slow eastward propagation of Tortugas eddies. However, to best of our knowledge, no observational and/or modeling study has reported the direct effect of the wind on the transport of the Yucatan Channel and Western Florida Strait as shown in Fig. 4.
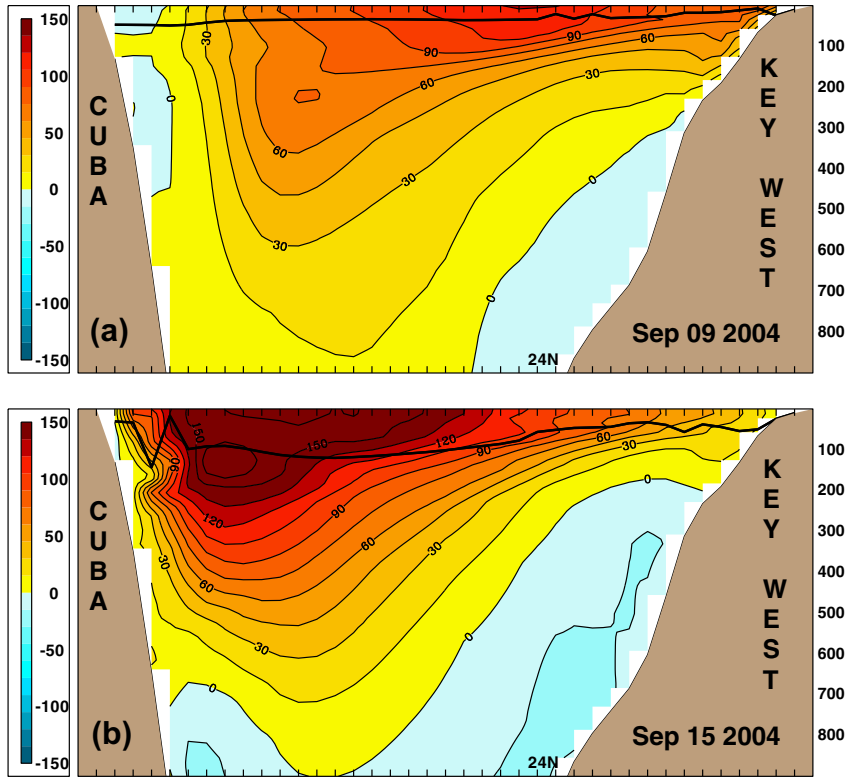
Fig. 3. East–West component of the velocity (color contours in cm/s) snapshots for September 9, 2004 (a) and September 15, 2004 (b) as simulated by the 1/25° nested GOM-HYCOM over a cross-section, which goes from Key West to Cuba and it is indicated with a blue line in Fig. 1. Positive currents indicate eastward flow. The mixed layer depth is represented by the black line.
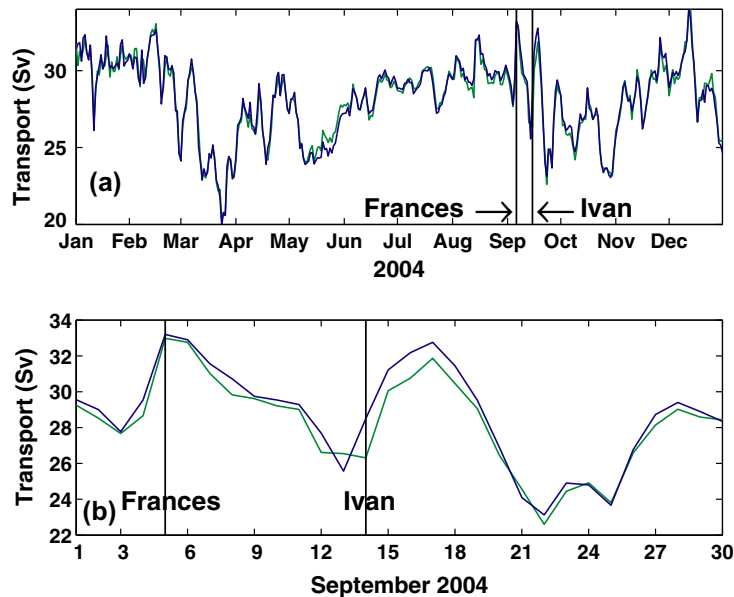

Fig. 4. Time series of transport (in Sv) simulated with 1/25° GOM-HYCOM over cross-sections along the Yucatan Channel (green line) and Key West–Cuba (blue line) for the complete 2004 (a), and for September 2004 (b). Positive transport indicates northward and eastward flow.

3.1.2. Coastally Trapped Wave generated by Hurricane Ivan along the coast of Cuba

The Hurricane Ivan wind field and its model ocean effects in the thermocline depth (in this study the depth

of the 20 °C isotherm is used as an indicator of the depth of the thermocline) and thermocline vertical velocity are presented in Figs. 5 and 6. Before the arrival of Ivan to the North Western Caribbean (September 10–11, 2004)
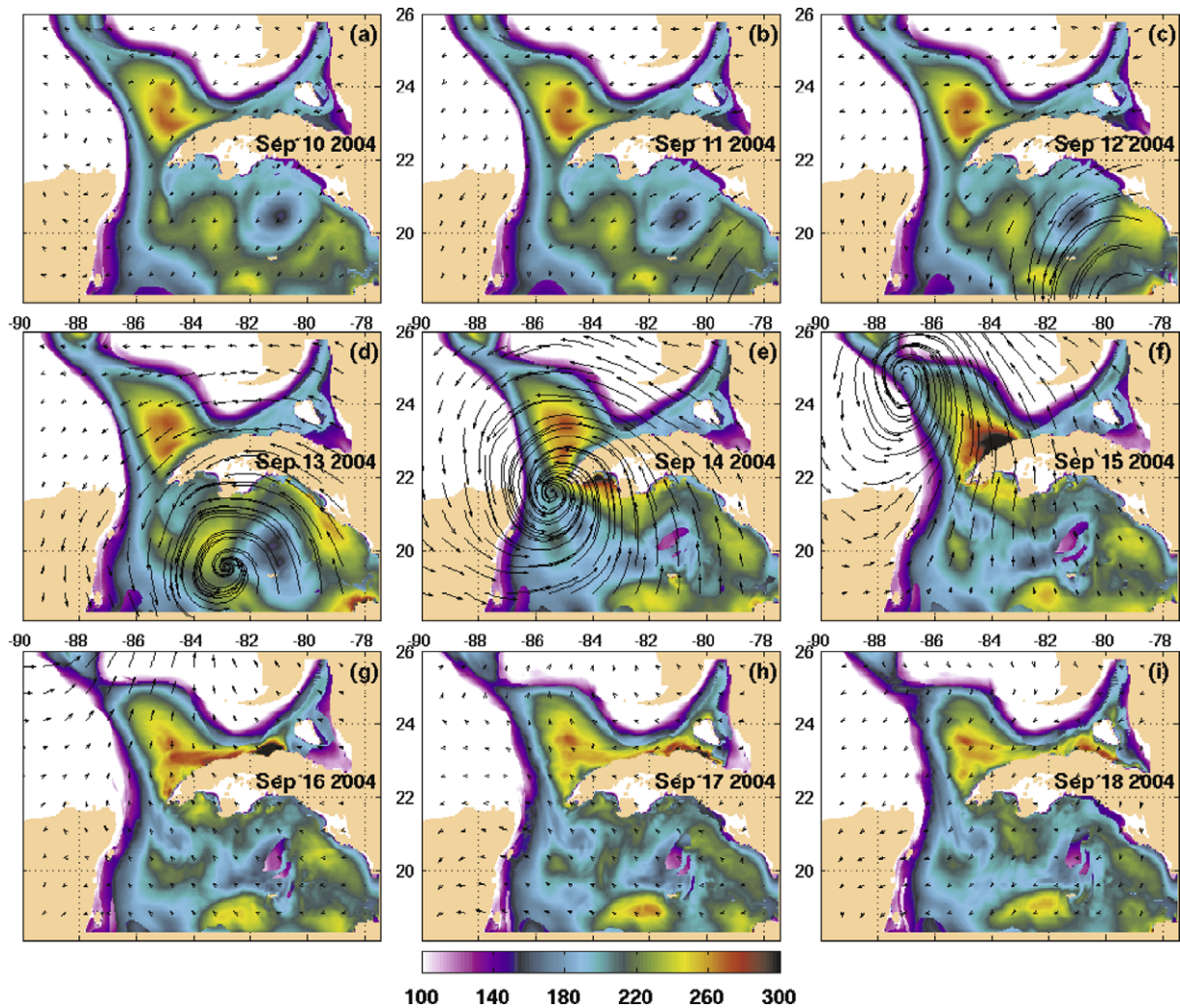
Fig. 5. Depth of the 20 °C isotherm (color contours in meters) over a GOM subregion for nine different dates in September 2004 as simulated by 1/25° GOM-HYCOM forced by NOGAPS 3-hourly winds (represented with curly vectors) and daily averaged thermal forcing. The different positions of the coastally trapped wave can be observed from September 12 (along the southeastern coast of Cuba) to September 18 (along the north-northeastern coast of Cuba).

the thermocline depth is characterized by a minimum and maximum of ~160 and ~270 m, respectively, which are associated with a cold-core cyclone centered close to 81°W, 20.5°N and with the Loop Current, respectively (Fig. 5a and b). In addition, the thermocline depth along the South Coast of Cuba is shallower than 180 m at this time. In general, during September 10 and 11 the thermocline's vertical velocity goes from 20 to 30 m/day in the North Western Caribbean. In particular, the area located between 82°W and 78.7°W and 18°N and 21°N is packed with distinctive semicircular bands, which are indicative of the incoming tropical system to the region (Figs. 6a and b). Also, no CTW can be recognized in the thermocline fields at this time (Figs. 5a, b and 6a, b). A day later (September 12) the frontal part of Ivan arrived to the region generating onshore Ekman transport and a strong coastal convergence, which deepened the coastal thermocline to ~250 m and produces a vertical velocity of >80 m/day along the southeastern coast of Cuba (Figs. 5c and 6c).

At the same time, the cold-core cyclone centered around 81°W, 20.5°N strengthens with the arrival of the frontal part of Ivan. During the next day (September 13) the cyclonic surface winds of Ivan continue driving the onshore Ekman transport, and consequently a coastal convergence that eventually generates a CTW along the southeastern coast of Cuba (Figs. 5d and 6d). This CTW is characterized by alongshore and cross-shore scales of ~230 km and ~100 km, respectively. Moreover, it is interesting to notice that even though this CTW is surface intensified, it has a deep structure. In fact, the presence of the CTW can be clearly observed in the 10 °C isotherm, which is close to 700 m deep along the coast of Cuba (not shown). Similar wind forcing prevailed through September 14 favoring coastal convergence and strengthening this Cuban CTW, which propagated along the south coast of Cuba as a wind-forced CTW at a propagation speed of ~4.4 m/s. A day later (September 15), this forced CTW partially rounded the western tip of the Cuban
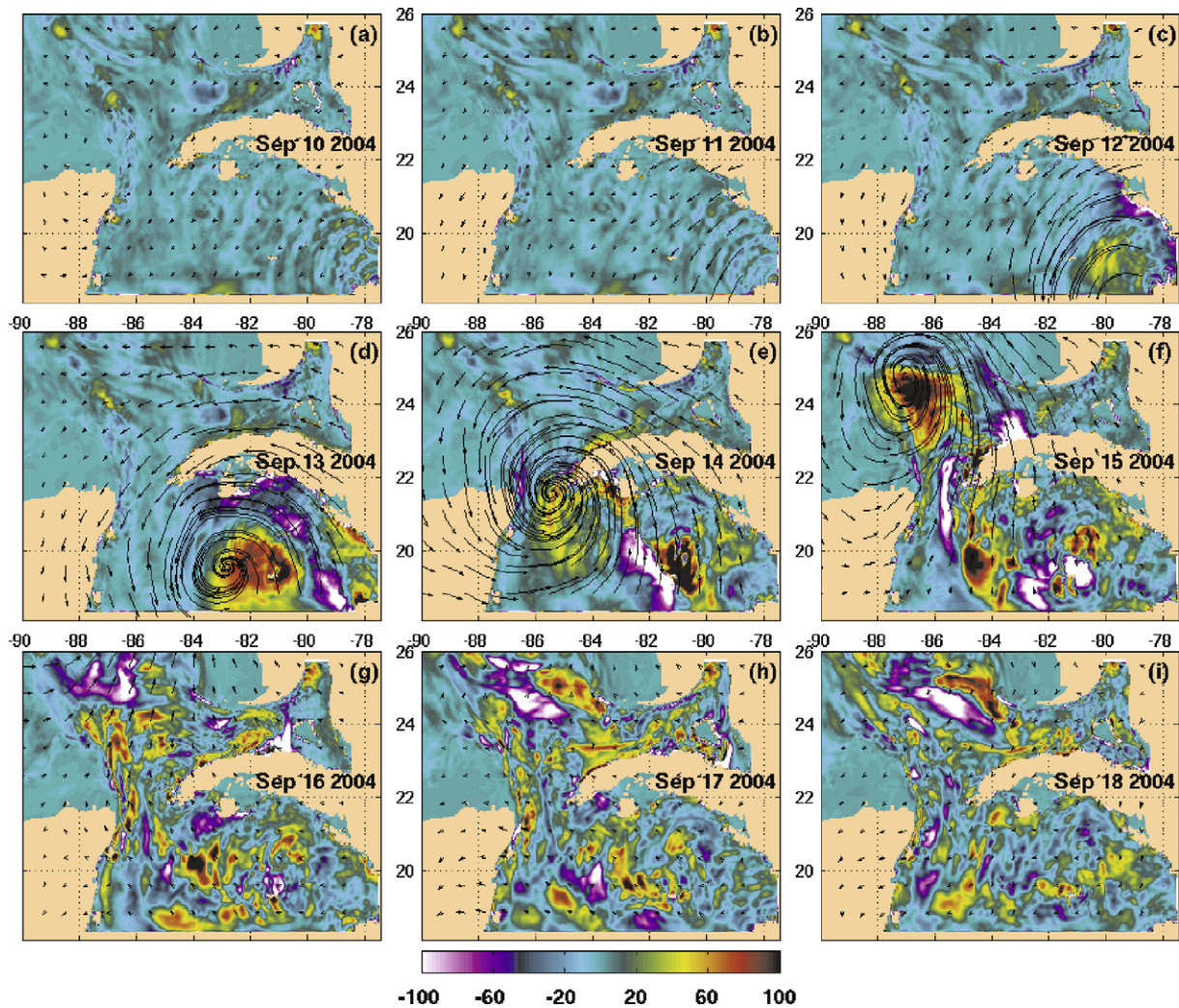
Fig. 6. Vertical velocity (color contours in meters/day) of the 20 °C isotherm over a GOM subregion for nine different dates in September 2004 as simulated by 1/25° GOM-HYCOM forced by NOGAPS 3-hourly winds (represented with curly vectors) and daily averaged thermal forcing.

Island. During its forced propagation along the northeastern coast of the Island, the CTW produces maxima in both thermocline depth (>300 m) and thermocline downwelling vertical velocity (>100 m/day) (Figs. 5f and 6f). Throughout the following three days (September 16–18) Ivan moves farther north of the Cuban Island (see Figs. 5g–i and 6g–i) allowing the wave to propagate along the northern coast of Cuba as a free CTW at the phase speed of ∼2.0 m/s, which agrees with the phase speed range of values reported in the articles reviewed by Brink (1991). Thus, while this CTW travels around most of the Cuban Island it exits the GOM nested domain at one of the nested open boundaries (Figs. 5g–i and 6g–i) showing the ability of the HYCOM boundary conditions to propagate strong signals out of the nesting domain. This finding complements the results of Zamudio et al. (2008) who demonstrated the capability of HYCOM open boundary conditions to propagate a CTW across a nesting boundary.

In the simulation and within the northwestern Caribbean, Ivan generated the strongest Ekman suction that raised the thermocline at a speed of ∼100 m/day, strengthened a cold-core eddy maximizing the cyclonic circulation (not shown), generated a cyclone surface cooling of ∼3 °C (not shown), and produced an upward displacement of the thermocline of ∼60 m at the center of the eddy (Figs. 5e and 6e). In agreement with this hurricane generated maximum cooling inside of a preexisting cold-core eddy, Walker et al. (2005) reported a wind speed reduction just after Ivan passed close to two cold-core eddies in the northern GOM. Since Ivan produced a maximum surface cooling in those two cyclonic eddies, the authors hypothesized that the cooling generated by Ivan provided an immediate negative feedback to Ivan's intensity. The upward displacement of the thermocline (Fig. 5) and the associated maximum surface cooling of the eddy close to 81°W, 20.5°N produced by the model (not shown), and Ivan's weakening from September 13 to September 14 (http://
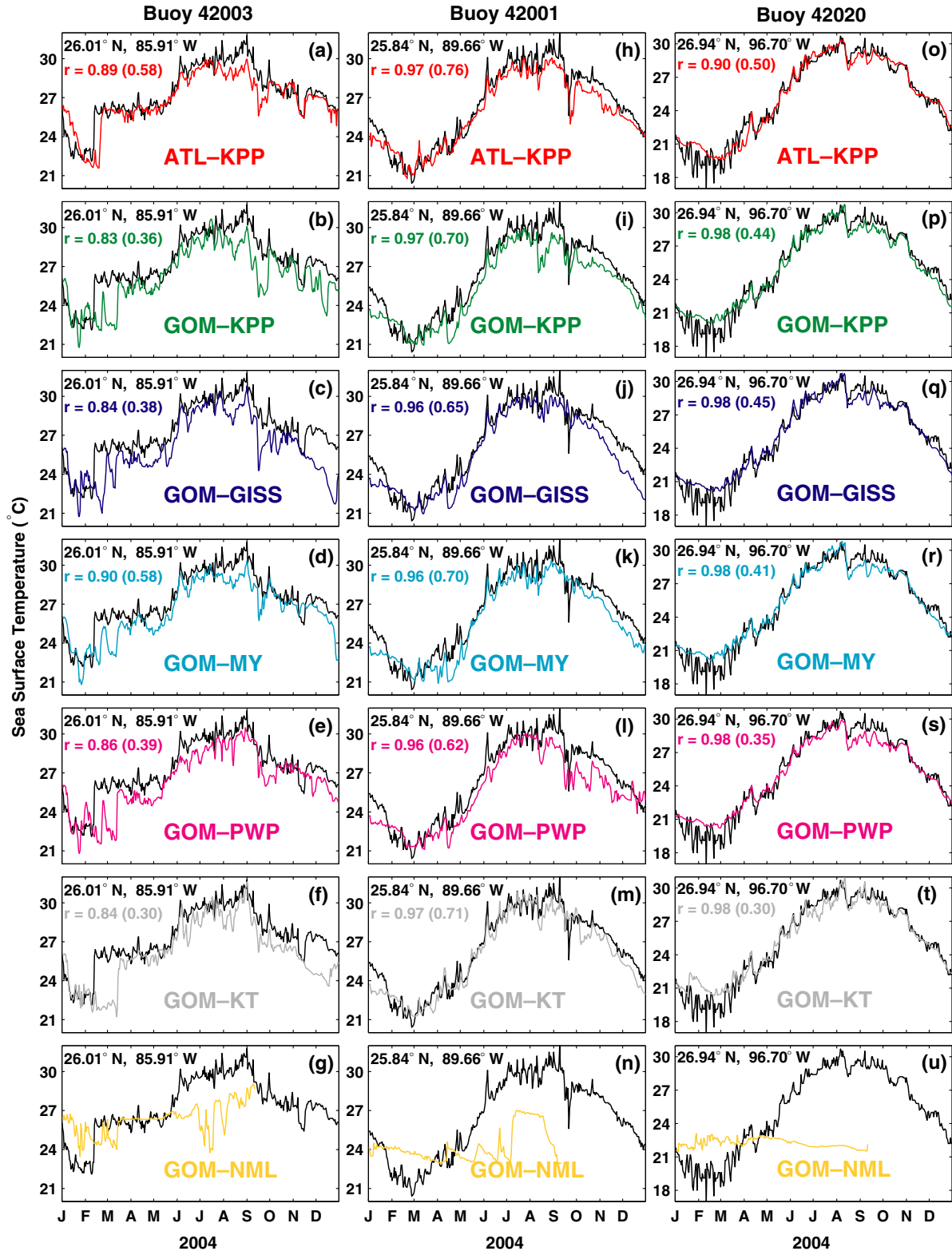
Fig. 7. Time series of observed (black line), and simulated (colored lines) sea surface temperature (in °C) on five different buoys on the Gulf of Mexico for 2004. The geographical locations of the buoys, the National Data Buoy Center (NDBC) station number, and the correlation coefficients (before and after (that is shown in parentheses) the removal of the annual cycle) between the observed and simulated time series are indicated. The abbreviations are as follow: ATL is the assimilative Atlantic HYCOM simulation, GOM is the non-assimilative regional Gulf of Mexico HYCOM simulations, KPP is the K-Profile Parameterization mixed layer model, GISS is the NASA Goddard Institute for Space Studies model, MY is the Mellor–Yamada mixed layer model, PWP is the Price–Weller–Pinkel mixed layer model, KT is for the Kraus–Turner mixed layer model, and NML is for no mixed layer.
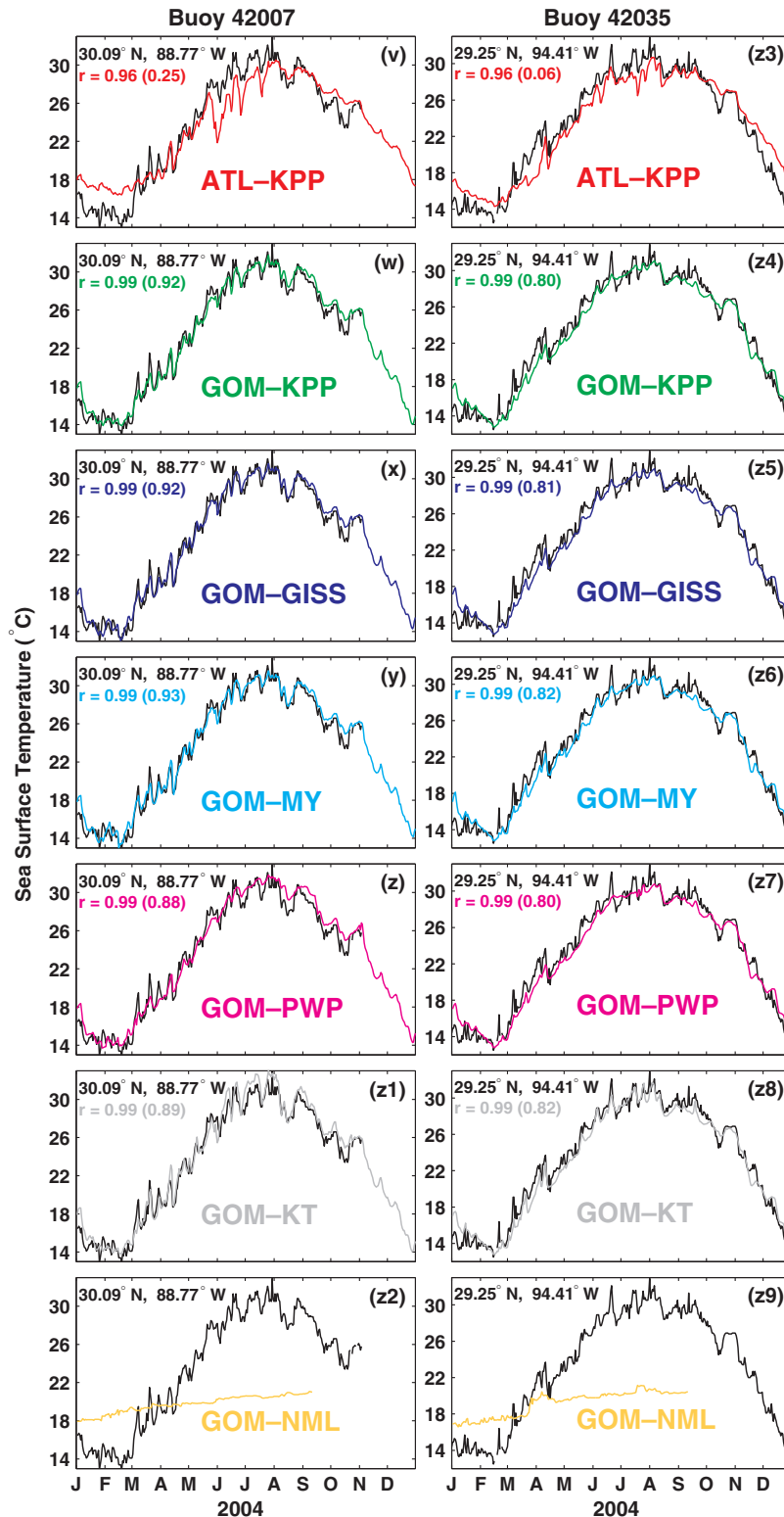
Buoy 42007 **Buoy 42035**

Fig. 7 (*continued*)

www.nhc.noaa.gov) just after passing to the west of the cyclonic eddy, are three facts which strengthen Walker's et al. (2005) hypothesis of immediate negative feedback to Ivan's intensity. However, this is not enough to prove the hypothesis of immediate negative feedback to hurricane's intensity, since the atmospheric model (NOGAPS) that provides the forcing is not coupled to the ocean model (GOM-HYCOM).
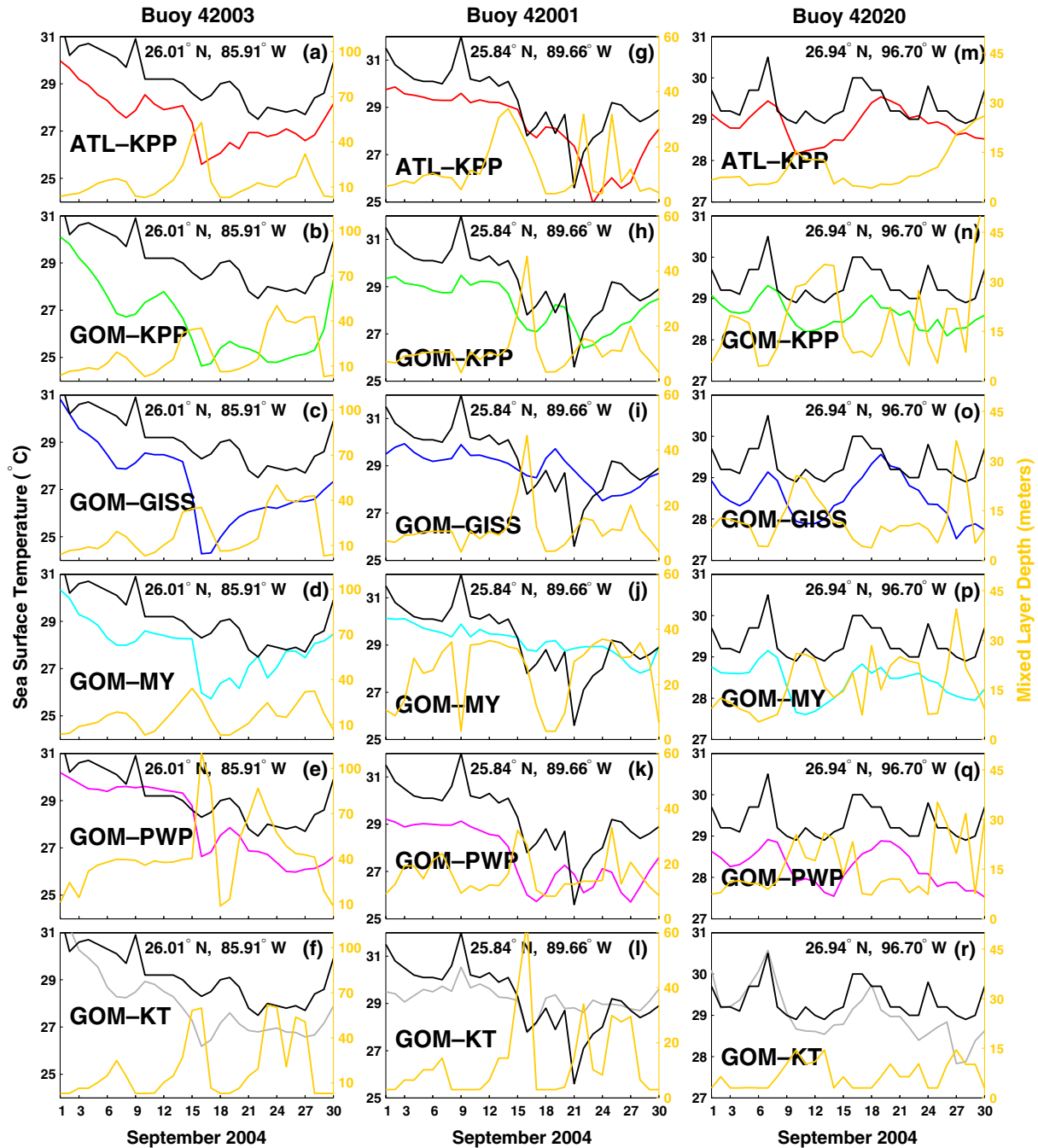
Fig. 8. Time series of simulated mixed layer depth (gold lines in meters) and observed (black line) and simulated (colored lines) sea surface temperature (in °C), on five different buoys on the Gulf of Mexico during September 2004. The geographical locations of the buoys and the National Data Buoy Center (NDBC) station number are indicated. The abbreviations are as follow: ATL is the assimilative Atlantic HYCOM simulation, GOM is the non-assimilative regional Gulf of Mexico HYCOM simulations, KPP is the K-Profile Parameterization mixed layer model. GISS is the NASA Goddard Institute for Space Studies model, MY is the Mellor–Yamada mixed layer model, PWP is the Price–Weller–Pinkel mixed layer model, and KT is for the Kraus–Turner mixed layer model.

3.2. Hurricane Ivan in the Gulf of Mexico

3.2.1. Sea surface temperature

SST measurements based on GOM buoys show an SST decrease of ~2–3 °C in 1–2 days as an upper ocean response to Ivan's winds (black lines in Figs. 7 and 8). Such strong and rapid ocean response to the hurricane wind forcing provides an excellent opportunity to examine the ability of mixed layer sub-models to simulate rapid cooling events. Thus, five different mixed layer sub-models were used to investigate the SST evolution during the year 2004, but we focus on September 2004, which is the Hurricane Ivan time frame. The implementation of the five different mixed layer sub-models in HYCOM has been
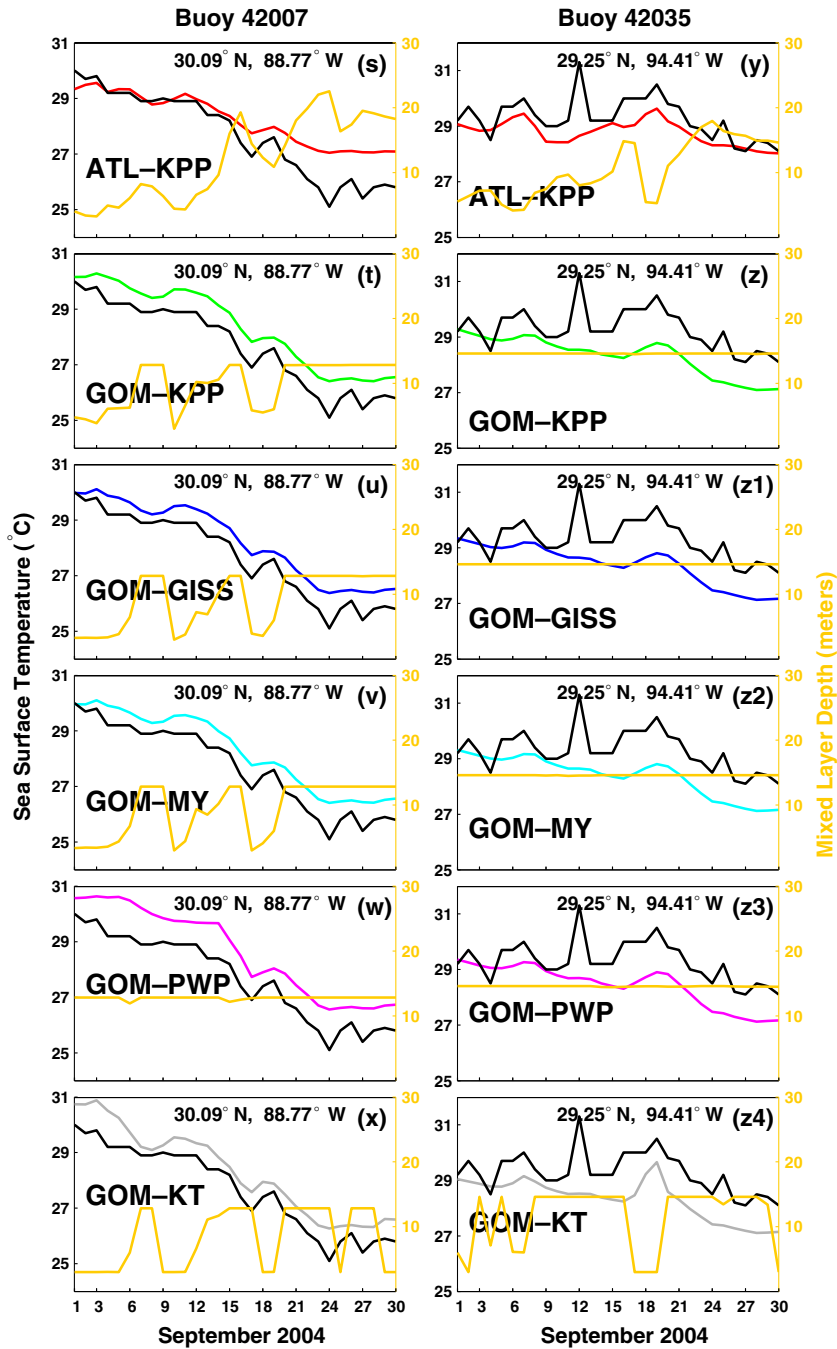
Fig. 8 (*continued*)

documented in Halliwell (2004) and in the HYCOM users Manual (Bleck, 2002, available at http://hycom.rsmas.mia-mi.edu/hycomodel/documentation.html). In general, the mixed layer sub-models provide HYCOM with the vertical eddy viscosity and diffusivity coefficients that reflect the vertical structure of the mixed layer. The three differential mixed layer sub-models embedded in the HYCOM are: the K-Profile Parameterization (KPP) model, which is characterized by vertical mixing from the surface to the bottom, the level 2 turbulence closure NASA Goddard Institute for Space Studies (GISS) model, and the 2.5 tur-bulence closure Mellor–Yamada (MY) model. In addition,

the two "slab" mixed layer sub-models, which are embed-ded in HYCOM are: the Kraus–Turner (KT) mixed layer model that is a vertically homogenized slab of water whose depth is diagnosed from the steady-state turbulence kinetic energy equation, and the Price–Weller–Pinkel (PWP), which is a quasi-slab dynamical instability mixed layer model.

Fig. 7 includes observed and simulated SST time series for the year 2004 at five different buoys located in the GOM. The basin scale model (which assimilate SST and SSH satellite data but does not assimilate any data mea-sured by the buoys) and the five non-assimilative regional
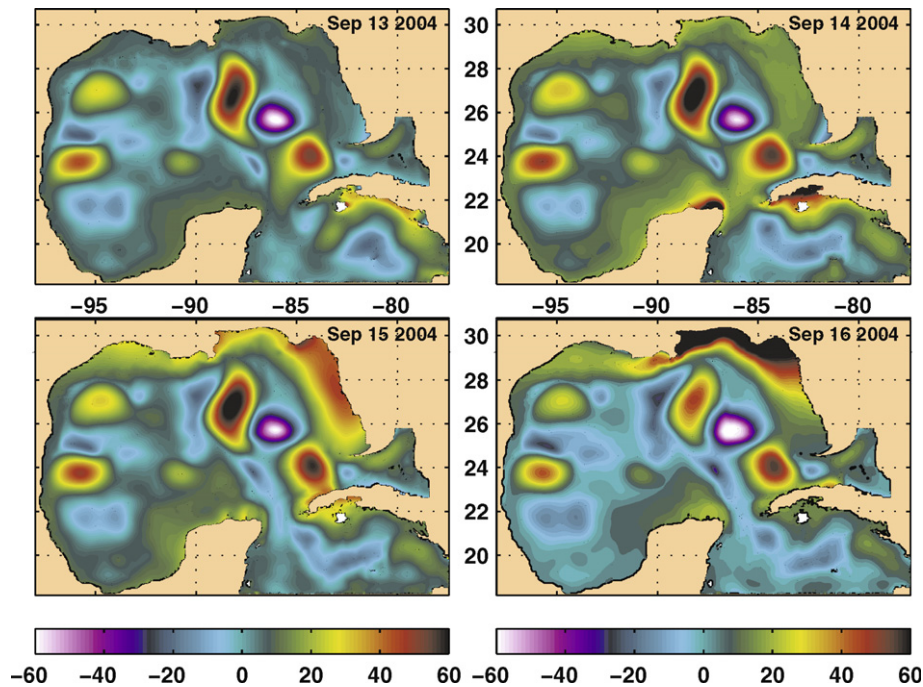
Fig. 9. Sea surface height anomaly (color contours in cm) for 4 different dates in September 2004 as simulated by 1/25° GOM-HYCOM forced by NOGAPS 3-hourly winds and daily averaged thermal forcing. The different positions of the coastally trapped wave can be clearly observed on September 15–16 along the coast of the GOM.

models with different mixed layer sub-models are able to simulate the observed SST with some success. Indeed, the correlation coefficients between the observed (represented by the black line) and simulated (represented by the colored lines) time series range from 0.83 to 0.99 (Fig. 7). These high correlations are due to the strong annual cycle of the GOM SST, as suggested by the reduction of the correlation coefficients, which range from 0.06 to 0.92 (Fig. 7), after the removal of the annual cycle from all the time series.

Before the removal of the annual cycle there is little difference in the SST simulated with the six different models. However, in the interior of the GOM and in the vicinity of the Loop Current, the basin scale model (which includes data assimilation) simulates the Loop Current and Loop Current eddies collocated with the observed ones. Consequently, this assimilative simulation is the one that more accurately agrees with the spatial fluctuations of the Loop Current. Two events generated by the spatial fluctuations of the Loop Current were measured by the two buoys that are more directly exposed to the Loop Current variability. The first event occurred during mid February 2004, and it increased the observed SST more than 2 °C in the buoy located at 26.01°N, 85.91°W as shown in Figs. 7a–f. Note that all the models include a delayed response to this observed SST jump. It is the assimilative basin scale (no-assimilative regional model including the KT mixed layer sub-model) model the one that simulate better (worse) the February 2004 observed SST jump (Figs. 7a–f). The second event is a cooling episode of approximately 3 °C, which occurred around September 21, 2004 in the buoy

located at 25.84°N, 89.66°W as shown by the black line in Figs. 7h, i and 8g, h. The ATL-KPP and GOM-KPP are the models that response most closely in phase to this observed SST cooling (Figs. 7h, i and 8g, h). In the particular case of the ATL-KPP model, the cooling event is also clearly reflected in the ~25 m increase in the mixed layer thickness as denoted by the gold line in Fig. 8g. In the case of the regional models, there are significant differences in the simulation of this cooling event. For instance, the GOM-KT model did not clearly incorporate the cooling event in the SST field, but it is the only regional model that clearly simulated a significant increase of more than 30 m in the mixed layer thickness, which is associated with the cooling event (at this time we do not have an explanation for this counter intuitive result). In addition, the GOM-KPP, GOM-GISS, and GOM-PWP models simulated partially this cooling event, and the GOM-MY model did not simulate the event at all.

Of particular interest for this study is the ~2–3 °C cooling induced by Ivan in the SST measurements of the buoys located at 26.01°N, 85.91°W and 25.84°N, 89.66°W during September 15–16, 2004. Note that the assimilative basin scale model (ATL-KKP) and all the regional models (with no ocean data assimilation or relaxation to any SST) response to the wind-forcing associated with Ivan, simulating the observed SST cooling (denote by the black and colored lines in Fig. 7a–m) and the mixed layer thickness increase (see gold lines in Fig. 8a–l). An unexpected and notable result is that the regional GOM-KT model is the only model (including the assimilative basin scale one),
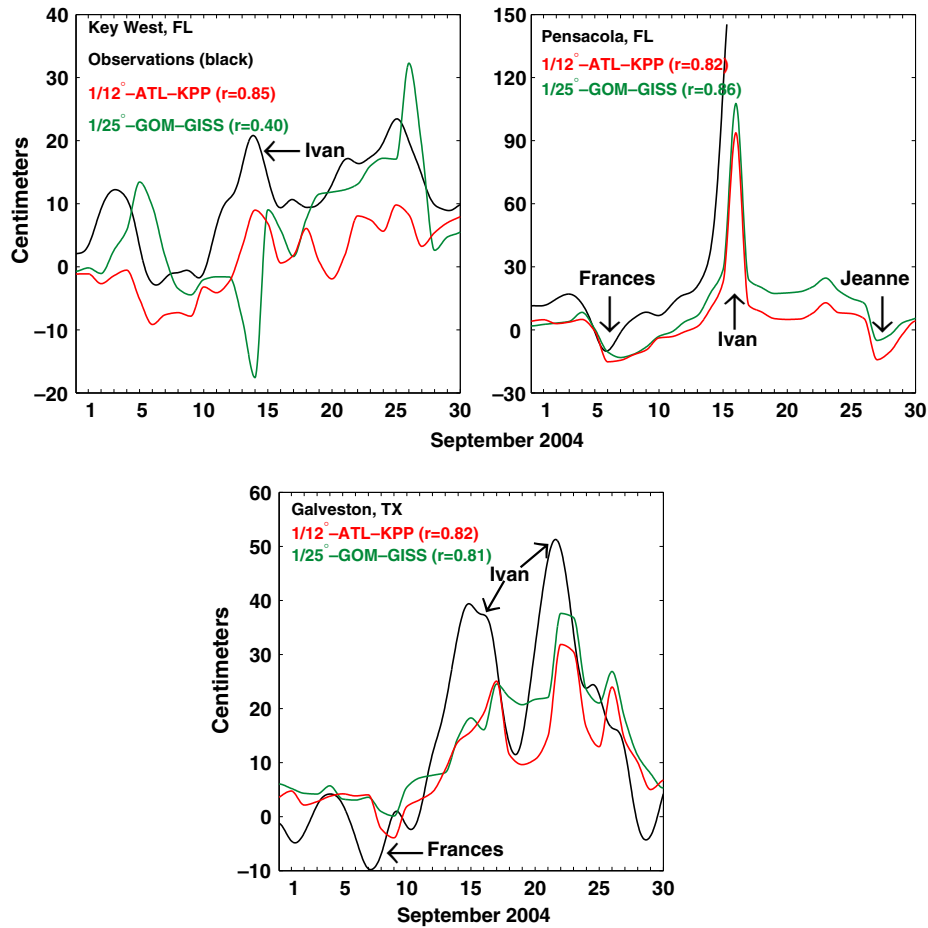
Fig. 10. Time series of observed (black line) and 1/12° Atlantic, and 1/25° GOM-HYCOM simulated (red, and green lines, respectively) sea surface height anomaly at Key West, FL, Pensacola, FL, and Galveston, TX. The observed data have been de-tided and corrected for atmospheric pressure loading effects. The correlation coefficient (r) between the observed and simulated time series is indicated for each of the three locations with red, and green for the 1/12° Atlantic, and 1/25° GOM-HYCOM, respectively.

which completely simulated the cooling event produced by Ivan during September 16, 2004 in the buoy of Fig. 8g–l. Why is that a surprising finding? Using basin-scale low resolution (2° zonal resolution and 2° cos (latitude) meridional resolution) climatological simulations, Halliwell (2004) evaluated the vertical mixing algorithms included in HYCOM and found that model performances deteriorates slightly when the KT slab mixed layer model is used. In contrast, based on the results shown in Fig. 8g–l and for the particular cooling event produced by Ivan, the performance of the high resolution (1/25°) simulations that are forced with 3-hourly winds improve slightly when the KT slab mixed layer model is used. However, based on this single case, this result can not be generalized. In fact, the correlation coefficients of Fig. 7 do not show significant difference among the regional models to be able to conclude dominance or insufficiency of any model. But it should be mentioned that a simulation without a mixed layer sub-model produces unrealistic SST, and blows up during Hurricane Ivan (Figs. 7g, n, u, z2, and z9), which shows the importance of the mixed layer for a proper simulation of high wind events.

After removing the annual cycle in the coastal waters of the northern GOM, the correlations between the measured and simulated time series indicate that the SST measured on the two buoys situated in shallow waters (Figs. 7v–z9 and 8s–z4) is significantly better simulated with all the regional models than with the basin scale model. A possible explanation for these large correlation coefficient differences (0.25 versus 0.88–0.93 for the buoy located at 30.09°N, 88.77°W and 0.06 versus 0.80–0.82 for the buoy located at 29.25°N, 94.41°W), is that the regional higher resolution model extends closer to the buoys than the lower resolution basin scale model does.

Overall, using as a quality criterion the correlation coefficient, the five mixed layer sub-models produce good results. Furthermore, based on the results of Figs. 7 and 8, under the direct influence of the Loop Current fluctuations, assimilation of satellite data can play a main role in the simulation of the SST variability. In contrast, in the shallow coastal waters of the northern GOM and far away from the direct influence of the Loop Current variability, model resolution can play a main role in the simulation of the SST variability.
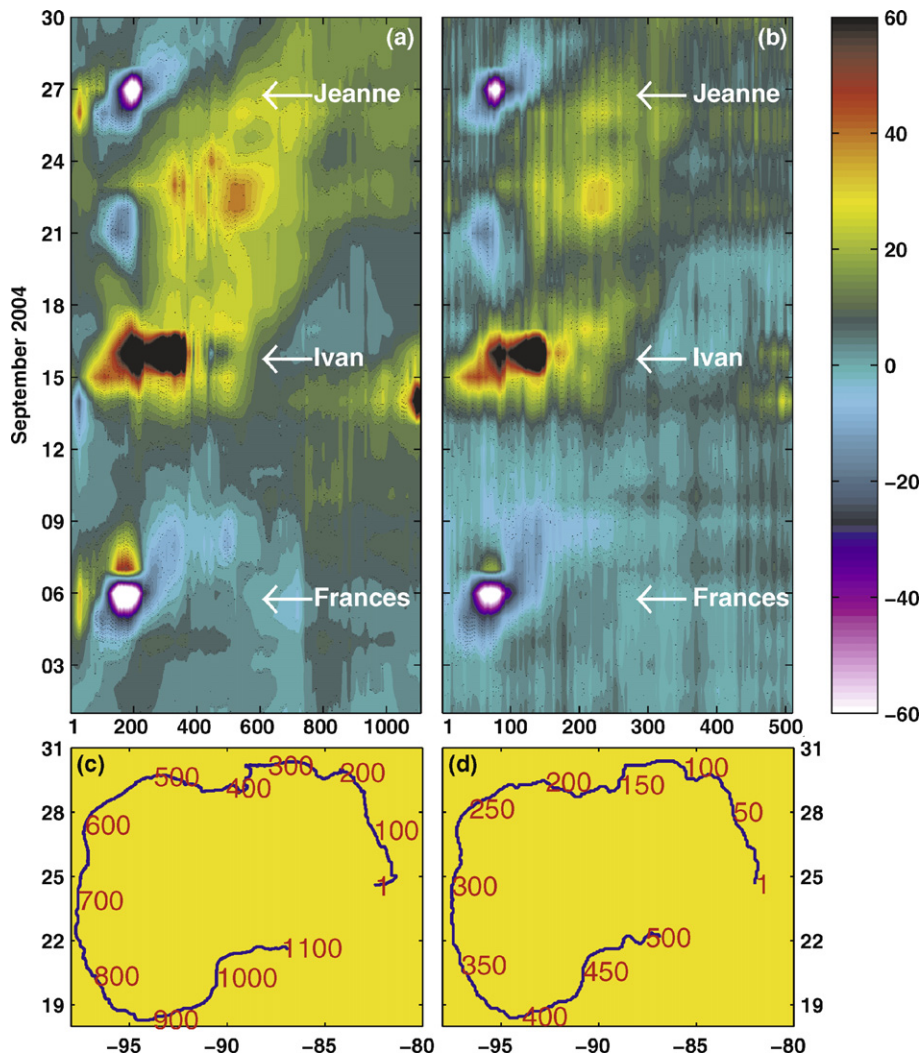
Fig. 11. Sea surface height anomaly time series simulated with (a) 1/25° GOM-HYCOM, and (b) 1/12° Atlantic HYCOM for September 2004 along the coast of the Gulf of Mexico. The different positions along the coast are indicated by the numbers that are shown in panels (c) and (d).

3.2.2. CTW generated by Ivan along the coast of the Gulf of Mexico

On September 14 2004 Ivan propagated through the Yucatan Channel entering to the GOM and its maximum sustained winds reduced from 71 m/s to 62 m/s (http://www.nhc.noaa.gov). The cyclonic open ocean response is featured by a vertical velocity of >100 m/day within the thermocline (Fig. 6f). The coastal ocean response along the Florida–Alabama–Mississippi–Louisiana coast is characterized by a forced CTW that starts to develop during September 14 reaching its peak on September 16 and raising the SSH >100 cm in the model and >140 cm in the sea level measurements at Pensacola, Florida (Figs. 9 and 10). This CTW has alongshore and across-shore scales of ∼700 and ∼80 km, respectively (Fig. 9). Fig. 11 includes two diagrams of along coastal SSH versus time as simulated by the regional GOM and the basin scale HYCOM. Although there are some differences between the coastlines of the regional and basin scale models (compare Figs. 11c and d), the two models clearly show the coastal signatures of Hurricanes Fran-

ces (September 6), Ivan (September 15–16), and Jeanne (September 27). Frances and Jeanne influenced the GOM after they were downgraded to tropical storms and forced the coastal waters of the GOM for only a few hours. Consequently, their relatively short period forcing generated only local non-propagating perturbations, which are displayed in the coastal-following SSH diagrams of Figs. 11a and b as negative SSH anomalies. In contrast, Ivan forced the waters of the GOM as a Hurricane and that forcing lasted ∼3 days. Thus, it generated a coastal downwelling signal that propagated as a forced CTW from Florida to Texas at a propagation speed of ∼10 m/s. However, this CTW was significantly weakened along the coast of Louisiana. How does this CTW weakened? Our explanation is as follows: The wave was generated and reinforced when Hurricane Ivan was located in the GOM and Ivan's downwelling favorable winds were blowing along the coast (Fig. 12, top). Later, when Ivan made landfall, upwelling favorable winds were blowing along the northern coast of the GOM weakening the CTW (Fig. 13, top). To isolate
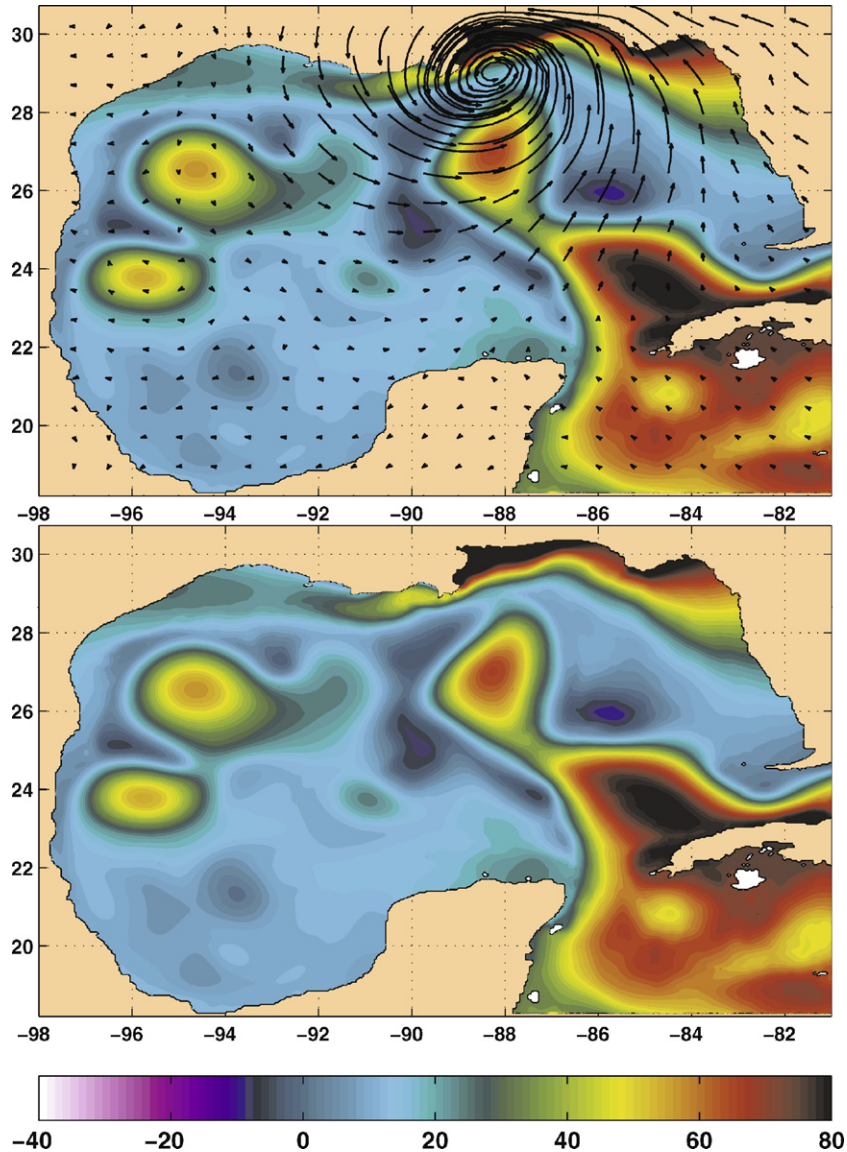
Fig. 12. Sea surface height anomaly (color contours in cm) for September 16, 2004 at 00 GMT as simulated by 1/25° GOM-HYCOM: (top) forced by NOGAPS 3-hourly winds and daily averaged thermal forcing (bottom) without including any forcing.

the wind effects in the weakening of this CTW, we performed a simulation running the GOM model without any wind forcing. The initial conditions for that unforced simulation include the CTW along the Florida–Alabama–Mississippi–Louisiana Coast (Fig. 12, bottom). Next, we allow the ocean model to evolve. An SSH comparison between the forced and unforced simulations clearly shows a difference of ∼25 cm in the SSH anomaly of the two CTW's propagating along the coast of Texas, the simulation with no wind forcing being the one which includes a CTW with higher SSH anomaly propagating along the coast of Texas (Fig. 13, bottom). Thus, this CTW was generated by Ivan's downwelling favorable winds along the coast of the GOM, but was subsequently greatly weakened by Ivan's upwelling favorable winds.

As this downwelling CTW propagated to the west, it generated alongshore westward currents. Those currents

combined with the currents forced directly by the hurricane winds produce alongshore westward currents of >2 m/s (Fig. 14a), which had a direct effect on both the alongshore and across-shore transport on the northern coast of the GOM (Fig. 14b). The two transport time series of Fig. 14b (which were sampled along the corresponding red and black lines of Fig. 14a) include predominantly eastward and northward flows that are in concordance with the climatological mean currents of the region (e.g. Smith and Jacobs, 2005). However, the mean eastward and northward flows are reversed by wind events of ∼2–4 days in duration, which appear mainly during fall-winter. These transport reversal events are less common during spring and summer, but during 2004 the largest transport reversal event was directly (wind induced currents) and indirectly (CTW associated currents) generated by Hurricane Ivan. The net model result was a westward transport of ∼8 Sv (note
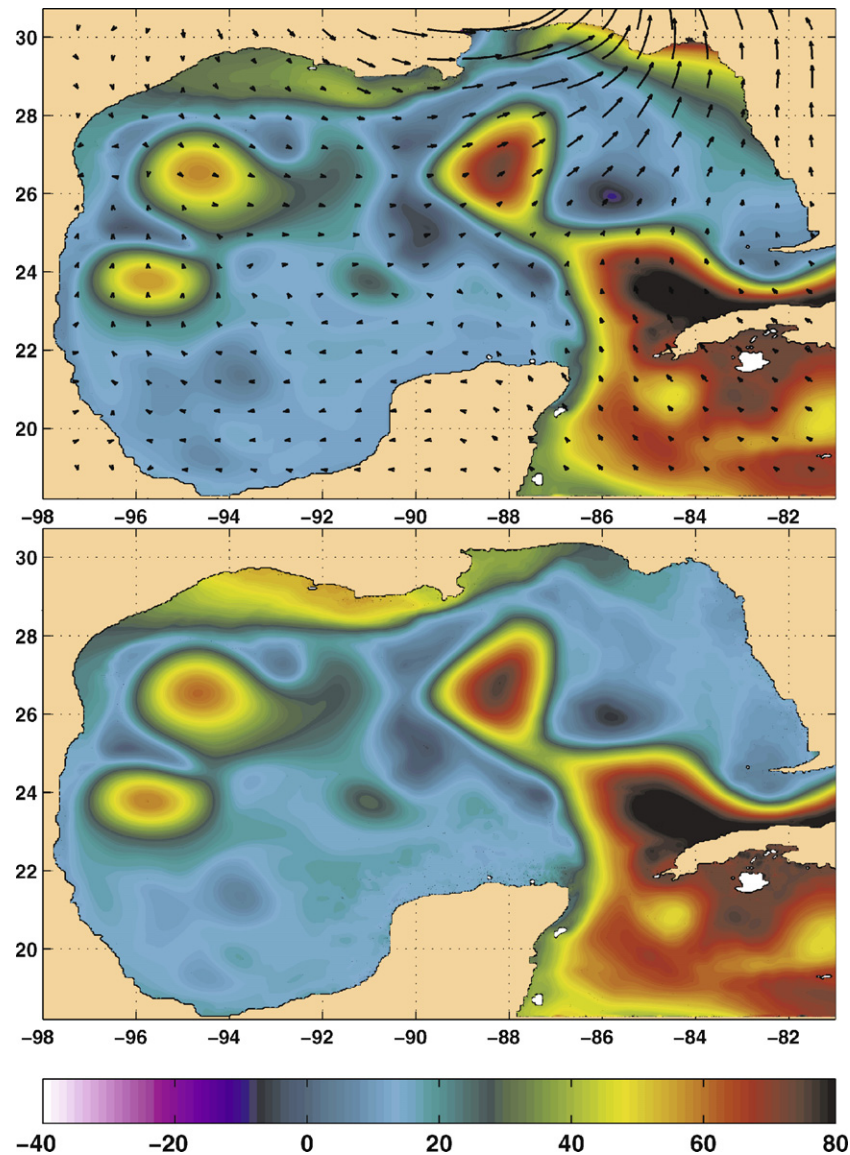
Fig. 13. Sea surface height anomaly (color contours in cm) for September 16, 2004 at 15 GMT as simulated by 1/25° GOM-HYCOM: (top) forced by NOGAPS 3 hourly winds and daily averaged thermal forcing (bottom) without including any forcing.

the mid September negative peak of the time series denoted by the black line in Fig. 14b) that was redirected to the south by Louisiana's coastline (as illustrated in Fig. 14a), generating a maximum southward transport of ~6 Sv (denoted by the red time series in Fig. 14b).

Fig. 10 shows a comparison between observed and modeled SSH at three different locations along the coast of the Gulf of Mexico. In the two locations along the Northern Coast of the Gulf (Pensacola and Galveston) both the regional model, which does not include any data assimilation, and the basin scale model (which includes assimilation of satellite measured SST and SSH but it does assimilate the SSH measured by the tide gauges) simulate very well (using as a quality criterion the correlation coefficient) the SSH variability during the two passes of Ivan but

underestimate the SSH amplitude. That is probably due, in part, to the 1° grid resolution of the atmospheric forcing (NOGAPS), which is not fine enough to simulate the small scale wind features generated by Hurricane Ivan (http://www.nhc.noaa.gov). In contrast, in the southern part of the Gulf (Key West) there are some important differences between the observed and regionally-simulated SSH. Several questions arise: Why is the regional model not able to simulate the SSH variability at Key West as successfully as in the case of Pensacola and Galveston? Why is the SSH variability simulated with the regional and basin scale models so different at Key West? In the following section we present evidences, which support that the SSH differences are probably due to the nondeterministic character of the currents in the region.

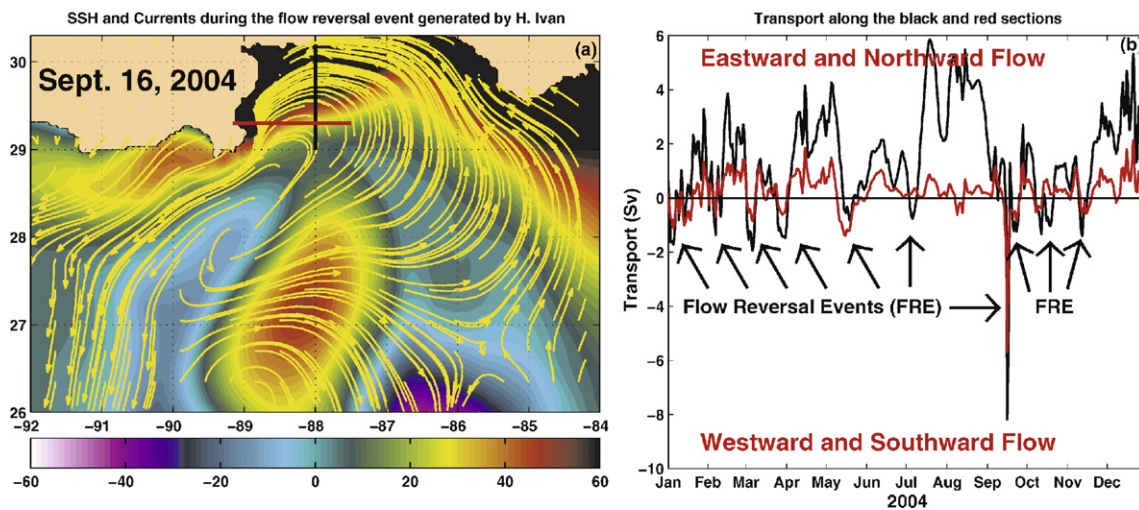## Flow Reversal Events along the Northern Gulf of Mexico

Fig. 14. (a) Sea surface height (color contours in cm) and currents (yellow curly vectors) for September 16, 2004 as simulated with 1/25° GOM-HYCOM. Time series of transport simulated over cross-sections along the red line from the Coast of Louisiana to 87.52°W, 29.31°N, and along the black line from the Coast of Mississippi to 88.00°W, 29.00°N (panel a). Positive transport indicates northward and eastward flow. The 10 flow reversal events of 2004 are indicated by the arrows.
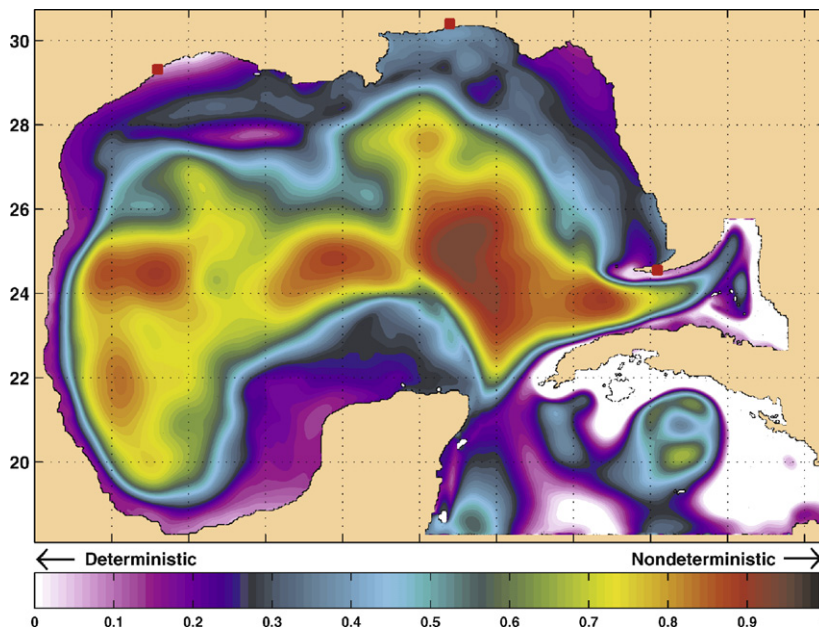

Fig. 15. Deterministic versus nondeterministic sea surface height variability for the GOM. Low and high values indicate high and low degree of determinism. These results are based on an ensemble of seven simulations forced with NOGAPS 3-hourly winds, which differ in the initial state only.

3.2.3. Deterministic versus nondeterministic variability in the Gulf of Mexico

In order to assess the degree of determinism in the simulations used in this study, two ensembles of seven simulations (in each ensemble) were integrated over the period 2004–2006. The seven simulations included in the first ensemble were forced with both local and remote forcing, and the seven simulations included in the second ensemble used remote forcing only (no wind forcing). In each ensemble the simulations differ only in their initial states (30 days apart). The initial conditions for the fourteen simulations of the two ensembles were interpolated from the basin scale model (ATL-HYCOM). Since these simulations differ only in initial state, any differences between them can be attributed to nondeterministic differences in both the initial conditions and the evolution of the simulations. Metzger et al. (1994), Metzger and Hurlburt (2000), Melsom et al. (2003), Hogan and Hurlburt (2005), and Zamudio et al. (2008) used a technique to separate the variability of a scalar variable into two components. The deterministic component is
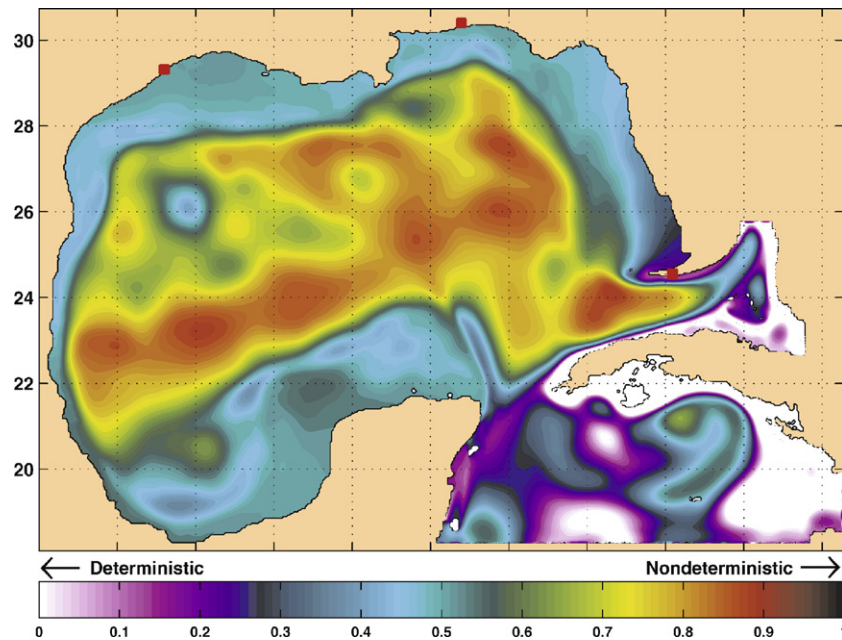
Fig. 16. Deterministic versus nondeterministic sea surface height variability for the GOM. Low and high values indicate high and low degree of determinism. These results are based on an ensemble of seven simulations, which do not include any wind forcing and they differ in the initial state only.

the direct response to the atmospheric forcing, the bottom topography and the coastline geometry, and the remote forcing, which in this case it is provided by the basin scale model through the boundaries of the regional nested model. The nondeterministic component is due to nonlinear mesoscale flow instabilities. The most important source of nonlinear mesoscale flow instabilities in the GOM are Loop Current intrusions, Loop Current Eddies (LCE) separation, and westward propagation of the LCE (Hurlburt and Thompson, 1980; Hurlburt et al., 1990). Since the LCE are generated without periodicity, but with an average separation time of 9.5 months and a separation time range from 3 to 21 months (Sturges and Leben, 2000; Zavala-Hidalgo et al., 2006). Then, the integration period was extended to 3 years to ensure adequate representation of LCE separation events. The 3-year period of integration permitted the generation of four LCE.

The technique of Metzger et al. (1994) is summarized as follows. First, the long-term mean (2004–2006) SSH is computed over the seven realizations. This mean is then removed from each daily record of the individual simulations to form seven time series of SSH anomaly fields (η). At each grid point, the temporally corresponding records of the seven realizations are averaged ($\bar{\eta}$) and deviations ($\eta' = \eta - \bar{\eta}$) are computed about the mean comprised of all realizations. These are then combined and averaged as follows:

$$\overline{\eta^2} = \bar{\eta}^2 + \overline{\eta'^2},$$

where the bar represents the average over all realizations. Averaging over the same period as the mean formed from all realizations, as was done here ensures that the temporal average of the deterministic anomalies is zero. Assuming $\bar{\eta}$ is accurately defined by a large number of realizations,

then, the left-hand side represents the total SSH variability and the right-hand side represents the SSH variability due to atmospheric, topographic, and remote forcings, plus the variability due to flow instabilities. Next, each component of the equation is divided by the total SSH variability ($\overline{\eta^2}$) to determine the fraction of the SSH variability due to either atmospheric–topographic-remote forcings or flow instabilities. Since the accuracy of this calculation depends on the number of ensemble members, then the fraction of variability was computed for 2, 3, 4, 5, 6, and 7 realizations. The quantitative and qualitative differences between the results of these calculations (maps) become progressively smaller as more simulations are included, and the relatively small difference between 6 and 7 realizations suggests convergence towards the mesoscale, and time scales.

The fraction of nondeterministic variability of SSH for the regional GOM model clearly shows the deterministic character of both the coastal regions, which is mainly due to the atmospheric forcing, and the open boundaries, which is due to the forcing provided by basin scale model (Fig. 15). Meanwhile, the nondeterministic characteristic of the Loop Current, LCE, and the path of the LCE is clearly displayed in Fig. 15. Note that the two buoys in the open GOM (where the assimilative basin scale model simulates the observed SST better than the non-assimilative regional models do) are located on the core of nondeterministic regions, whereas the three coastal buoys (where the regional models simulate the observed SST better than the basin scale model does) are located in deterministic regions. In addition, the three tide gauges stations (Key West, Pensacola, and Galveston) are located inside of deterministic regions, but the tide gauge at Key West is clo-

ser to nondeterministic regions as indicated by Fig. 15, suggesting a larger influence of nondeterministic signals on the tide gauge at Key West than at the tide gauges at Pensacola and Galveston. This nondeterministic effect is reflected in the poor SSH (using as a quality criterion the correlation coefficient between observed and simulated SSH) simulated with the regional model, but not in the SSH simulated with the basin scale model, because this last simulation includes assimilation of satellite measured SSH, which acts as a SSH constrain/forcing and the regional simulations are non-assimilative ones.

To test the hypothesis that the wind is the most significant forcing of the deterministic variability along the coasts, the ensemble of the seven simulations of Fig. 15 was repeated, but now each of the seven simulations was integrated over the period 2004–2006 without any wind forcing (Fig. 16). Thus, all the differences between Figs. 15 and 16 can be attributed to the atmospheric forcing. A comparison of Figs. 15 and 16 highlight the deterministic signal forced by the wind along the coastal regions. For instance, as expected the coastal areas dominated by the deterministic signals decrease significantly from Figs. 15 and 16. However, the nondeterministic character of the open GOM prevails in the simulation forced without any wind forcing, since it is primarily forced by the Loop Current, LCE, and the path of the LCE and not by the local wind. Also, note how the coastal tide gauge stations change from deterministic regions, in the ensemble with wind forced experiments (Fig. 15), to nondeterministic regions in the ensemble with non wind forcing experiments (Fig. 16), suggesting the importance of the local wind as a forcing of deterministic variability in coastal regions.

4. Summary and concluding remarks

The ocean response to Hurricane Ivan is studied using a 1/25° grid resolution GOM configuration of HYCOM that is nested inside of an eddy-resolving (1/12° equatorial resolution) North Atlantic configuration of HYCOM. The nested GOM approach allows direct examination of the connectivity of the GOM with the North Atlantic Ocean at high resolution and relatively low computational cost and permits the free propagation of hurricanes and hurricane generated signals (like eddies and currents) from the Atlantic to the Caribbean and from the Caribbean to the GOM. Model results indicate that during its passage over the North Western Caribbean, Ivan's along-coast winds forced an oceanic onshore Ekman transport generating a strong coastal convergence along the southeastern coast of Cuba. The convergence depressed the thermocline ~100 m, induced a vertical velocity within the thermocline of ~100 m/day, and generated a CTW along the southeastern coast of Cuba. Subsequently the CTW propagated along the southern coast of Cuba as a forced CTW and partially circumvented the western tip of the Cuban Island to continue its propagation along the northern Coast of Cuba as an unforced CTW leaving the nesting domain by one of the two open eastern boundaries. The visualization and discovery of this CTW are in part due to the high horizontal grid resolution (1/25°) and high frequency output (3 h) used in the regional GOM nesting models, since these two features are computationally too expensive to be used regularly in basin-scale models. At the same time, in the North Western Caribbean, Ivan rose the thermocline at the speed of ~100 m/day, produced a surface cooling of ~3 °C in a pre-existing cold-core eddy, and weakened its winds just after passing to the west of the cyclonic eddy. These three features strengthen Walker's et al. (2005) hypothesis of immediate negative feedback to Ivan's intensity. Later, the direct effect of the wind on the transport along the Yucatan Channel resulted on a transport's increment of ~2 Sv/day.

During its passage over the GOM Ivan's winds increased the mixing and upwelling reducing the SST >3 °C along Its path. That cooling effect was clearly measured by the buoy of Fig. 8l and simulated by the five different mixed layer sub-models, which are embedded in HYCOM. A modest but important SST result is that the SST variability measured with the two buoys situated on shallow waters is simulated with more accuracy (higher correlation coefficient) by the regional GOM model than by the basin scale model (Fig. 7). That could be an evidence of the advantages of using higher resolution models to simulate the process in shallow waters. Along the coast, Ivan's westward winds raised the SSH >140 cm on the tide gauge at Pensacola, Florida generating a second CTW along the coast of Florida–Alabama–Mississippi–Louisiana, but this wave was subsequently greatly weakened by Ivan's eastward winds. Another oceanographic processes generated by Ivan is that the northern coast of the GOM is characterized by 10–12 transport reversal events per year (Fig. 14). Those events are more common during fall and winter, however Ivan generated the largest transport reversal event of 2004. Finally, the analysis of deterministic versus nondeterministic variability shows that an important fraction of the SSH variability along the GOM coasts can be attributed to the local wind forcing, while the nondeterministic variability becomes more important in the interior of the GOM and in the vicinity of the Loop Current.

computer code used to extract the model points along the coast. The sea level data was obtained from the publicly accessible web site (http://uhslc.soest.hawaii.edu) at the University of Hawaii Sea Level Center and sea surface temperature data was obtained from the publicly accessible web site (http://www.ndbc.noaa.gov/) of the National Data Buoy Center. This paper is NRL contribution number NRL/JA/7320-07-7185. Thanks are extended to Dr. Alan Wallcraft (Naval Research Laboratory) for his contribution in the development and custody of HYCOM, and to two anonymous reviewers for their constructive comments, suggestions, and corrections, which greatly improved the manuscript.

References

Bleck, R., 2002. An oceanic general circulation model framed in hybrid isopycnic-cartesian coordinates. Ocean Modell. 37, 55–88.

Bleck, R., Benjamin, S.G., 1993. Regional weather prediction with a model combining terrain-following and isentropic coordinates. Part 1: Model description. Mon. Weather Rev. 121, 1770–1785.

Brink, K.H., 1991. Coastal-trapped waves and wind-driven currents over the continental shelf. Ann. Rev. Fluid Mech. 23, 389–412.

Bunge, L., Ochoa, J., Badan, A., Candela, J., Scheinbaum, J., 2002. Deep flows in the Yucatan Channel and their relation to the Loop Current extension. J. Geophys. Res. 107 (C12), 3233. doi:10.1029/2001JC00125.

Canuto, V.M., Howard, A., Cheng, Y., Duvovikov, M.S., 2001. Ocean turbulence. Part I: one-point closure modell. Momentum and heat vertical diffusivities. J. Phys. Oceanogr. 31, 1413–1426.

Canuto, V.M., Howard, A., Cheng, Y., Duvovikov, M.S., 2002. Ocean turbulence. Part II: vertical diffusivities of momentum, heat, salt, mass, and passive scalars. J. Phys. Oceanogr. 32, 240–264.

Chassignet, E.P., Arango, H., Dietrich, D., Ezer, T., Ghil, M., Haidvogel, D.B., Ma, C.C., Mehra, A., Paiva, A.M., Sirkes, Z., 2000. DAMEE-NAB: the base experiments. Dyn. Atmos. Oceans 32, 155–184.

Chassignet, E.P., Hurlburt, H.E., Smedstad, O.M., Halliwell, G.R., Hogan, P.J., Wallcraft, A.J., Baraille R., Bleck, R., 2007. The HYCOM (HYbrid Coordinate Ocean Model) data assimilative system. J. Marine Syst. in press, doi:10.1016/j.jmarsys.2005.09.016.

Halliwell, G.R., 2004. Evaluation of vertical coordinate and vertical mixing algorithms in the HYbrid-Coordinate Ocean Modell (HYCOM). Ocean Modell. 7, 285–322.

Hamilton, P., Larsen, J.C., Leaman, K.D., Lee, T.N., Waddell, E., 2005. Transports through the Straits of Florida. J. Phys. Oceanogr. 35, 308–322.

Hogan, P.J., Hurlburt, H.E., 2005. Sensitivity of simulated circulation dynamics to the choice of surface wind forcing in the Japan/East Sea. Deep Sea Res. II 52, 1464–1489.

Hurlburt, H.E., Thompson, J.D., 1980. A numerical study of Loop Current intrusions and eddy-shedding. J. Phys. Oceanogr. 10, 1611–1651.

Hurlburt, H.E., Fox, D.N., Metzger, E.J., 1990. Statistical inference of weakly correlated subthermocline fields from satellite altimeter data. J. Geophys. Res. 95, 11375–11409.

Johns, W.E., Lee, T.N., Beardsley, R.C., Candela, J., Limeburner, R., Castro, B., 1998. Annual cycle and variability of the North Brazil Current. J. Phys. Oceanogr. 28, 103–128.

Kara, A.B., Wallcraft, A.J., Hurlburt, H.E., 2005a. A new solar radiation penetration scheme for use in ocean mixed layer studies: An application to the Black Sea using a fine resolution HYbrid Coordinate Ocean Model (HYCOM). J. Phys. Oceanogr. 35, 13–32.

Kara, A.B., Wallcraft, A.J., Hurlburt, H.E., 2005b. How does solar attenuation depth affect the ocean mixed layer? Water turbidity and atmospheric forcing impacts on the simulation of seasonal mixed layer variability in the turbid Black Sea. J. Clim. 18, 389–409.

Kara, A.B., Wallcraft, A.J., Hurlburt, H.E., 2005c. Sea surface temperature sensitivity to water turbidity from simulations of the turbid Black Sea using HYCOM. J. Phys. Oceanogr. 35, 33–54.

Large, W.G., McWilliams, J.C., Doney, S.C., 1994. Oceanic vertical mixing: a review and a model with a nonlocal boundary layer parameterization. Rev. Geophys. 32, 363–403.

Lee, T.N., Leaman, R., Williams, E., Berger, T., Atkinson, L.P., 1995. Florida Current meanders and gyre formation in the southern Straits of Florida. J. Geophys. Res. 100 (C5), 8607–8620.

Mellor, G.L., Yamada, T., 1982. Development of a turbulence closure model for geophysical fluid problems. Rev. Geophys. Space Phys. 20, 851–875.

Melsom, A., Metzger, E.J., Hurlburt, H.E., 2003. Impact of remote oceanic forcing on Gulf of Alaska sea levels and mesoscale circulation. J. Geophys. Res. 108 (C11), 3346. doi:10.1029/2002JC00174.

Metzger, E.J., Hurlburt, H.E., Jacobs, G.A., Kindle, J.C., 1994. Hindcasting wind-driven anomalies using reduced-gravity global ocean models with 1/2° and 1/4° resolution. NRL Tech. Rep. 9444, Nav. Res. Lab., Stennis Space Center, MS, p. 21.

Metzger, E.J., Hurlburt, H.E., 2000. The nondeterministic nature of Kuroshio penetration and eddy shedding in the South China Sea. J. Phys. Oceanogr. 31, 1712–1732.

Niiler, P.P., Kraus, E.B., 1977. One-dimensional models of the upper ocean. In: Kraus, E.B. (Ed.), Modelling and Prediction of Upper Layers of the Ocean. Pergamon, New York, pp. 143–172.

Price, J.F., Weller, R.A., Pinkel, R., 1986. Diurnal cycling: observations and models of the upper ocean response to diurnal heating, cooling, and wind mixing. J. Geophys. Res. 91, 8411–8427.

Rosmond, T.E., Teixeira, J., Peng, M., Hogan, T.F., Pauley, R., 2002. Navy operational global atmospheric predictions system (NOGAPS): forcing for ocean models. Oceanography 15 (1), 99–108.

Schott, F.A., Fischer, J., Reppin, J., Send, U., 1993. On mean and seasonal currents and transport at the western boundary of the equatorial Atlantic. J. Geophys. Res. 98 (C8), 14353–14368.

Sheinbaum, J., Candela, J., Badan, A., Ochoa, J., 2002. Flow structure and transport in the Yucatan Channel. Geophys. Res. Lett. 29, 1040. doi:10.1029/2001GL01399.

Smith, S.R., Jacobs, G.A., 2005. Seasonal circulation fields in the northern Gulf of Mexico calculated by assimilating current meter, shipboard ADCP, and drifter data simultaneously with shallow water equations. Cont. Shelf Res. 25, 157–1834.

Sturges, W., Leben, R., 2000. Frequency of ring separations from the Loop Current in the Gulf of México: a revised estimate. J. Phys. Oceanogr. 30, 1814–1819.

Turner, J.S., Kraus, E.B., 1967. A one-dimensional model of the seasonal thermocline II: the general theory and its consequences. Tellus 19, 98–105.

Walker, N.D., Leben, R.R., Balasubranian, S., 2005. Hurricane-forced upwelling and chlorophyll a enhancement within cold-core cyclones in the Gulf of Mexico. Geophys. Res. Lett. 32, L18610. doi:10.1029/2005GL02371.

Wang, D.W., Mitchell, D.A., Teague, W.J., Jarosz, E., Hulbert, M.S., 2005. Extreme waves under Hurricane Ivan. Science 305, 896.

Willebrand, J., Barnier, B., Böning, C., Dieterich, C., Killworth, P.D., LeProvost, C., Jia, Y., Molines, J.-M., New, A.L., 2001. Circulation characteristics in three eddy-permitting models of the North Atlantic. Prog. Oceanogr. 48, 123–161.

Zamudio, L., Hogan, P.J., Metzger, E. J., 2008. Summer generation of the Southern Gulf of California eddy train. J. Geophys. Res. in press, doi:10.1029/2007JC004497.

Zavala-Hidalgo, J., Morey, S.L., O'Brien, J.J., Zamudio, L., 2006. On the Loop Current eddy shedding variability. Atmósfera 19, 41–48.